Spacecraft Anomaly Forecasting Using Heterogenous Environment Data

Laila Andersson, Lars Eliasson,
Jian-Guo Wu, Henrik Lundstedt, Peter Wintoft

IRF Scientific Report 264

October 1999

ISSN 0284-1703

Institutet för rymdfysik

Swedish Institute of Space Physics

Kiruna, Sweden

Spacecraft Anomaly Forecasting Using Heterogenous Environment Data

Laila Andersson, Lars Eliasson,
Jian-Guo Wu, Henrik Lundstedt, Peter Wintoft

IRF Scientific Report 264
October 1999

Institutet för rymdfysik
Swedish Institute of Space Physics

Kiruna, Sweden

IRF Scientific Report 264
ISSN 0284-1703

Swedish Institute of Space Physics
Box 812
SE-981 28 Kiruna
SWEDEN
www.irf.se

STUDY OF PLASMA AND ENERGETIC ELECTRON ENVIRONMENT AND EFFECTS

ESTEC/Contract No. 11974/96/NL/JG(SC)

99-10-27

TECHNICAL NOTE, WP 230

SPACECRAFT ANOMALY FORECASTING USING HETEROGENOUS ENVIRONMENT DATA

Authors
Laila Andersson, Lars Eliasson
Swedish Institute of Space Physics, Box 812, SE-981 28 Kiruna, Sweden

Jian-Guo Wu*, Henrik Lundstedt, Peter Wintoft
Swedish Institute of Space Physics, Solar-Terrestrial Physics Division
Scheelevägen 17, SE-223 70 Lund, Sweden.

* Now at Danish Meteorological Institute
Lyngbyvej 100, DK-2100 Copenhagen O, Denmark

ESA Technical Officer:
A. Hilgers, Space Environments and Effects Analysis Section (TOS-EMA)
ESA Technological Research Programme Space Environments and Effects
Major Axis

Page left free intentionally

TABLE OF CONTENTS

DOCUMENTATION CHANGE RECORD

Issue	Rev.	Sect.	Date	Changes
Draft	0.1	All	980321	Presentation at PM5
	0.2	All	980517	Presentation at PM6
	1.0	All	980529	Submitted to ESTEC for approval
Final	1.1	All	990319	Revised version
	1.2	All	991027	Second revision, mainly editorial

1 Introduction

1.1 Purpose of this document

This document is the final technical report of the study "Spacecraft Anomaly Forecasting Using Heterogeneous Environment Data" (WP 230) that is part of a subcontract under "Study of plasma and energetic electron environment effects." More information about the activities under this contract can be found on internet (http://www.geo.fmi.fi/spee). The report summarises and gives references to work on space environment monitors and our experience using local and non-local environment data to forecast spacecraft anomalies.

1.2 Main objective

Energetic solar particles, other high-energy radiation, and the local plasma environment form a hazardous environment to Earth-orbiting satellites and interplanetary probes. More and more everyday functions rely on satellite operations, sensitive instrumentation and/or manned flights. Therefore, the knowledge of the plasma and energetic particle effects, reliable forecast methods, advanced tools and reliable databases have become increasingly important.

This study is intended to improve the knowledge on how the space environment influences spacecraft, primarily in geostationary orbit. Some anomaly records and environment data sets are used to determine when there is an increased risk for spacecraft anomalies. The main objective is to forecast anomalies combining local and non-local environment data. Predictions based on either local or non-local data have been presented in other technical reports (SPEE-WP210 and SPEE WP-220).

Satellite anomalies caused by space weather effects are, e.g., on-board computational errors, communication failures, satellite system shut-downs, position errors or errors in satellite orientation. Spacecraft anomalies can be classified into two major classes; single event upsets (SEUs) (Robinson et al., 1994) and anomalies caused by discharges (Violet and Frederickson, 1993). Spacecraft discharges can be external or internal to the spacecraft.

The seasonal dependence of anomalies and their relation to, e.g., the South Atlantic magnetic anomaly, solar activity, and geomagnetic activity has been reported by, e.g., Wilkinson, (1994). The most significant charging events are found in low-density plasmas, low altitude auroral oval passes and during high solar activity. A more detailed discussion on the different types of anomalies is given in Section 2.

The use of sensitive electronic components and the need to keep the weight of the spacecraft at a minimum increase the possibility that a satellite will be affected in an unwanted way by

the space environment. Many ground-based and airborne systems today rely on satellite information. To forecast periods with increased risk for anomalies is therefore important. In Sections 3 and 4 different environment monitors and the availability of environment data are described.

In Section 5 different forecast models are presented. The results from these models are used in Section 6 to propose a satellite anomaly index, that can be used by satellite operators to give a warning when there is an increased risk of anomalies. Finally, some recommendations for future space environment monitors are given.

1.3 Forecasts

Up to now the space environment has mainly been analysed based on data with low resolution. Analysis using simple models have given useful solutions for some applications but the demands have increased with the development of new electronic components and more sensitive systems/instruments. New mechanisms generating anomalies have been identified and previously overlooked or disregarded types of radiation can now, for some applications, cause anomalies. Therefore, one needs to take into account other energy ranges than those included in earlier models. There is also a need to further investigate the physics behind these effects.

A forecast can be made for a specific spacecraft or for a more general situation. It can be based on on-board sensors after a short in-flight calibration period or other environment data. The threshold value for a satellite is typically unknown beforehand but reasonable estimates can be made.

The forecast tool should be easy to use. It should give a warning when the environment conditions are likely to cause problems to satellite systems. The threshold for a warning depends on the satellite position and sensitivity. Some satellites experience almost no anomalies, while others have anomalies more frequently. Even if the spacecraft never has had an anomaly, during harsh conditions it can suddenly be affected. Even if the spacecraft operators do not take any precaution, they are made aware that something can happen and can react in a more efficient way. The operators can also avoid complicated commanding, e.g., thruster firings when a warning is given.

The environment conditions are different in geostationary orbit (GEO), low Earth orbit (LEO), geostationary transfer orbit (GTO) and in interplanetary orbits. For instance the latitude and longitude are important in LEO orbits. For GEO the longitude and latitude are of less importance.

A useful forecast model must not only forecast hazardous conditions that can cause anomalies but also give a low number of false alarms. The system should also be able to give correct warnings as early as possible, so that appropriate actions can be taken.

2 Satellite anomalies

A spacecraft anomaly can be caused by, e.g.:

- outgassing from satellite systems
- the neutral thermosphere drag
- deep dielectric charging
- surface charging
- meteoroids and spacecraft debris
- solar radiation, cosmic rays
- geomagnetic phenomena
- energetic particles in the radiation belts.

Some of these are often correlated, so the exact cause of an anomaly is sometimes difficult to determine (James et al., 1994). Spacecraft charging, high-energy particle impact, and debris are the three main causes of anomalies. We have assumed that anomalous behaviour caused by errors in commanding or software is excluded from the lists of anomalies.

During 1993-95 twenty environmentally induced severe anomalies on-board NASA Goddard spacecraft were reported (Goddard Space Flight Center, 1994, Remez and McLeod, 1996 and Walter, 1995). For the Goddard spacecraft more than 400 reported anomalies occurred during these 3 years of operation but most of them could be identified either as part of the process of learning to control the spacecraft or as single event upsets (SEUs) from single high energy particles. Sometimes anomalies can occur due to the RF environment (Leach and Alexander, 1995). NOAA-11 was affected by spurious commands due to a noisy VHF-communication. On NOAA-12 spurious commands occurred when the vehicle flew over commercial VHF-disturbances in Europe. NOAA maintains a spacecraft anomaly data base (Wilkinson, 1994). There are several internet sites containing information about the space environment and its effects on satellites.

2.1 Causes

2.1.1 Outgassing and UV-light

During the first period after launch there is a significant outgassing when the spacecraft enters vacuum conditions. Sudden increases of the pressure locally can cause a discharge that can give rise to anomalies. Exposure to UV-light above the atmosphere can change the properties of materials and cause anomalous behaviour.

2.1.2 The neutral environment

Neutral particles exist also far outside the Earth's magnetopause. Chemical interaction (mainly atomic oxygen) and large drag forces occur at low altitudes where the particle

densities are high. Solar events can lead to sudden increases in atmosphere densities that disturb the satellite attitude and orbit. This might lead to a decrease of the spacecraft lifetime. These effects are mainly important for low-altitude orbits and therefore not further discussed in this report.

2.1.3 Plasma interactions

Charges accumulated on spacecraft surfaces (e.g., Garrett, 1981; Garrett and Whittlesey, 1996) can cause potential differences that can impact spacecraft systems through arcing. A discharge can occur between the surface and the surrounding space plasma, between different parts on the surface, or inside materials of the satellite. A current spike, during discharge, can generate electromagnetic radiation that can penetrate the spacecraft and/or damage the surface and electronics directly. Discharges at the edges of solar cells are common (Tribble, 1995).

Potentials can be generated by the **v** x **B** force, depending on the spacecraft size and the local plasma density. Other sources are currents to and from the spacecraft such as photoelectron emission, auroral electron beams, hot plasma injections during magnetic storms or auroral substorms. Charges mainly accumulate at sharp edges. The amount of charging depends on the surface properties, such as material resistivity and secondary emission yield.

In low-altitude orbits outside the auroral region, the level of negative surface charging is usually small (less than 10 V). On auroral field lines spacecraft charging may become 100 V negative or more. Negative voltages above 1 kV can occur (Garrett and Whittlesey, 1996) due to, e.g., auroral electron beams (Stevens and Jones, 1995). The strongest charging events appear when the spacecraft is in eclipse and in a region with reduced thermal ion density. A spacecraft in LEO moves through a relatively dense plasma at a velocity exceeding the thermal velocity of the ions but lower than the velocity of the electrons.

Spacecraft in GEO, Medium Earth Orbit (MEO) or Highly Elliptical Orbit (HEO) can be charged to high voltages causing discharges and other disturbances. A magnetic storm enhances the possibility of charging. There is a strong seasonal and daily variation in the occurrence frequency of spacecraft discharges because of eclipse periods and magnetospheric structure and dynamics. For example, the GOES spacecraft spurious commands occurred between 23 and 08 local time. There are often anomalies for GEO spacecraft during equinox (spring and fall) due to eclipse periods.

2.1.4 Radiation

High-energy particles can penetrate the surface, interact with the material, and deposit the energy in the interior of the spacecraft. How the energy is deposited and what kind of

interactions that takes place depends on the radiation type (photon, electron, ion, or neutral particle), the energy of particles and the material where the energy is deposited.

High-energy radiation can charge dielectric material to the electric field breakdown level by electron deposition. If charges accumulate inside capacitors (with a slow decay time) radiation induced dielectric charging can occur (Frederickson, 1980). Radiation can also cause lattice damage, disrupting currents in devices and thus degrade instruments and other spacecraft systems.

Radiation through semiconductors causes electron-hole pairs along the path. If the total dose is high enough the component can fail.

Events following a single high-energy particle impact are called single event phenomena (SEP) or single event effect (SEE) (http://flick.gsfc.nasa.gov/radhome/papers/seespec.htm). They are normally caused by heavy ions. There are three classes of SEP: "single event upset" (SEU), "single event latch-up" and "single event burnout" (SEB) (Hastings, 1995). SEU is a change in the state of a digital circuit due to an energetic particle (cosmic ray or proton). A single event latch-up occurs when, instead of a bit flip a spurious current path created by the high-energy particle draws a large current, the circuit hangs and a reset has to be made. An SEB occurs when the circuit fails permanently due to the charge cloud created by the high-energy particle. A difference between SEE and spacecraft charging is that a SEE only need one particle of high energy to cause the malfunction whereas spacecraft charging needs many.

Single event upsets on LEO satellites are often related to the South Atlantic Anomaly (SAA). Trapped protons and cosmic rays causing SEU are anti-correlated with solar activity. The SEU probability depends on the sensitive area (Lauriente and Vampola, 1996) and to the types of electronic devices.

Solar radiation effects can be forecasted a few hours or days in advance but the flux magnitude, duration and heavy ion composition is difficult to forecast.

2.1.5 Dust and debris interaction

At geostationary distances the main debris are of natural origin. In low-earth orbit the population of man-made micrometer debris are comparable to natural particles. Depending on density, relative velocity and size debris can contaminate spacecraft, puncture insulators or even completely demolish satellites. Small debris can puncture the surface without directly damaging the spacecraft. Small-sized particles impacting on surfaces charged by plasma interactions can initiate a discharge.

Meteor showers can cause problem to satellite operation. Not necessarily a meteoroid making a hole in the satellite, but rather, from the creation of a plasma, or free electric charge on the spacecraft. The charge can cause damage to sensitive electronic circuits on board the spacecraft, and ultimately cause the spacecraft to fail. The first assumed case of a satellite being lost by a meteoroid came in 1993. The Olympus communications satellite was reported being damaged by a meteor strike (1993 Perseid meteor shower) and was lost as a result of an electrical failure. The ESA press release from 26 August tells. "As indicated in the press release of 17 August, 1993, service from the Agency's experimental OLYMPUS satellite was interrupted during the night of 11/12 August when, for reasons which are not yet understood, the satellite lost earth pointing attitude and began spinning. This event, and the subsequent recovery actions, used the last few kilograms of fuel remaining on the satellite. An assessment of the situation indicated that it would be impossible to re-establish service. It has therefore been decided that the Olympus mission should be terminated and the satellite removed from the geostationary orbital ring."

2.2 Local time and orbit dependence

The types of anomalies vary with orbit (Vampola, 1994). The space environment is very different in different orbit types. For example a solar proton event can enhance the radiation belt particle fluxes 2 Re from Earth and be observable for several months (Daly et al., 1994). Geomagnetic storms often follow solar events such as coronal mass ejections. As a result energetic particles are injected into the magnetosphere. The radiation belt particles can move in the radial direction and this way cause dropouts at GEO or enhanced fluxes with time delays if compared to geomagnetic activity in other regions of the magnetosphere.

In geostationary orbit high level surface charging often occurs near midnight local times. Deep dielectric charging occurs often in early afternoon local time. SEUs mainly occur when a solar proton event is in progress or due to cosmic rays. The transition between shadow and sunlight conditions modifies surface charging due to photo-emission effects. Surface charging is also often associated with the auroral oval.

In low-altitude polar orbit the most pronounced SEUs occur at high latitudes and at the South Atlantic anomaly. The South Atlantic anomaly is a very dangerous region for SEUs.

Anomalies are not only reported from satellites in Earth orbit. The Voyager spacecraft reported anomalies (internal electrostatic discharges) during the passage of Jupiter. These discharges appear to have resulted from high-energy electron flux (above 10 MeV). The Pioneer spacecraft encountered severe space weather conditions in the Jovian radiation belts, which nearly destroyed some on-board systems.

Examples of anomalies that have occurred on spacecraft in different orbits are given in Table 1. The anomalies range from harmless to total loss of spacecraft.

Table 1. *Some reported spacecraft anomalies*.

Spacecraft	Time	Comment	Reference
DSP		Anomalies associated with >1.2 MeV electrons	Vampola, 1994
SCATHA		Internal discharges associated with outer radiation belt	Garrett and Whittlesey, 1996
ATS 5 and ATS 6		Charged to 10 kV in eclipse at GEO	SMASS Report
NOAA spacecraft	from 1971	Contains 2779 events from 1971to 1988	Wilkinson, 1994
Goddard spacecraft	1993-1995	More than 400 anomalies	Remez and McLeod, 1996; Walter, 1995
Voyager 1		Power-on resets	Leung et al., 1986
Pioneer		Severe space weather near Jupiter	SMASS Report
GPS		Clock shift, false commands	James et al., 1994
Intelsat 3 and 4		Spin up	James et al., 1994
GOES 2			Lauriente et al., , 1996, 1998
GOES 3		Upsets	
GOES 4	Nov 26, 1982	Instrument failed on arrival of 110-500 MeV protons	Vampola 1994
Intelsat K	Jan 20 1994	Loss of attitude control in GEO	Baker et al. 1994
ANIK E1 and ANIK E2	Jan 20-21 1994	Loss of attitude control due to high energy electrons	Baker et al. 1996
ANIK E1	Mar 26 1996	Array of solar power panels disconnected	ISTP Newsletter, Vol 6, no 2, 1996.
DRA-delta		Phantom commands	Wrenn and Sims, 1996
CTS		Short circuit	James et al., 1994
DSCS II		Spin up, amplifier gain	James et al., 1994
DMSP 7		Charged to 300 V in less than a second- associated with a sharp drop in ion density	Stevens and Jones, 1995
GOES 5	July 22 1984	Failure during high energetic electron fluxes	Baker
DMSP F13		Problems while passing through an aurora	Anderson and Koons, 1996
Hispasat 1A and 1B	Sep 1992 and July 1993		Selding, 1998
Telstar 401	Jan 11 1997	Failure probably due to coronal mass ejection	Anselmo, 1997
Telstar 402		Spacecraft charging	Lanzerotti et al., 1996
Topex/Poseidon		Failures due to electrostatic discharges and SEUs caused by high energy protons	Lauriente and Vampola 1996
Intelsat 511	Oct 7 1995	Lost Earth lock	http://www.astro.lu.se/~henrik/spacew4b.html
GOES 8	Feb 14 1995	Attitude control difficulty	http://www.astro.lu.se/~henrik/spacew4b.html
TDRSS 1	1988-1991	SEUs anticorrelated with solar cycle	Wilkinson 1994
CRRES	1990	674 reported anomalies	Violet & Frederickson 1993
Tempo 2	11 Apr 1997	Temporary power fluctuations.	http://www.seds.org/spaceviews/970515/tech.html
Olympus	11/12 Aug 1993	Affected by the 1993 Perseid meteor shower?	See 2.1.5 above

2.3 The space environment

During recent years it has become clear (Reames, 1995) that solar proton events are caused by coronal mass ejections (CMEs). Earlier models divide the solar cycle into a quiet and an active period. During the quiet period no proton events are statistically expected to happen. However, a proton event occurred on 3-9 November 1997, i.e. during the minimum of the solar cycle 22 (Daly, 1997). Gabriel et al., (1996) introduced a new method of forecasting proton events, besides the statistical method used for JPL-91. They use an intelligent hybrid system, a so called neurofuzzy system, with X-ray flux as input and proton flux as output. Today, forecasting a proton event is very much a question of how to predict CMEs and to relate the characteristics of the CME to the proton flux. The ESA/NASA satellite SOHO has given us a very powerful tool to predict CMEs. Halo CMEs are easily forecasted from either the LASCO or EIT instrument on board SOHO. The fastest CMEs shock the solar wind plasma ahead of the CME producing energetic proton events.

Galactic Cosmic Rays (GCR) have very low fluxes but their high energy and mass can strongly ionize matter. They can reach sensitive parts and cause upsets at a microscopic scale. Anomalous cosmic rays result from charge-exchange between solar wind and interstellar neutral gases. The Earth's magnetic field provides some protection to spacecraft from solar and galactic ions.

During strong magnetic storms the magnetopause can move closer to the Earth so that satellites in GEO are located outside and in a completely different plasma environment.

The radiation belts encircle the Earth, an inner belt containing mainly energetic protons of up to several hundred MeV energy and an outer belt containing mainly energetic electrons up to a few MeV. The outer belt is highly dynamic, being subject to magnetic storms and particle injections. The inner belt extends to a geocentric radius of about 4 Re and the outer to about 10 Re. Injection events occurring in the outer radiation belt are also associated with the injection of hot plasma into the near-earth magnetosphere (causing auroral substorms). These injections can cause electrostatic charging of spacecraft surface materials leading to discharges.

Electrons are being accelerated at altitudes between about 1-2 Re to energies above 10 keV on field lines connected to the auroral ovals. These high-intensity electron fluxes can also cause spacecraft charging.

The cold and dense plasmas at low altitudes interact in a number of ways with space systems, e.g., current flows from exposed high-voltage parts, electrodynamic interactions of tethered

systems, and electromagnetic noise. Plasma-spacecraft interactions in the cold plasma environment can also cause problems.

Small solid particles, space debris, meteoroids and dust are an increasing threat to space systems. Ground-based optical and radar techniques can give information on objects above about 1 cm in diameter. For evaluating effects from meteoroids and debris below that limit, statistical models are used. Some planetary missions (with, e.g., landers) will have to deal with the problems of dust. This is also the case for missions to comets (e.g. Rosetta) and asteroids.

2.4 Spacecraft design

Most spacecraft are designed to have the interior shielded from the surrounding plasma and a wide variety of protections against anomalies. These include shunt diodes for protecting solar cells, filters and diodes to prevent discharges from influencing internal and components and circuits which are SEU and discharge resistant (Kalweit, 1981) and/or constructed with error corrections and latch-up protection.

To avoid potential differences conducting materials are used. If dielectric materials are on the outside they are usually coated with e.g., indium tin oxide (Garrett, 1981).

In some scientific experiments active control of potential is established using ion or electron gun.

Spacecraft have been launched with a smaller spacecraft attached by a fibre. These tethered spacecraft are designed to interact with the plasma environment for current generation or thrust, in some cases simply to probe the properties of the plasma.

3 Local environment monitors

3.1 Space instruments

3.1.1 Particle detectors

There are several types of particle instruments for neutral atom and/or charged particle (electron and ion) measurements. Different techniques are used to separate the unwanted species from the particles that are to be detected. Light (photons) from the Sun and the Earth's atmosphere must also be taken into account and stopped from entering into sensors. Particles with high energy can interact or penetrate instrument walls and cause background counts that can make the data interpretation more difficult or even impossible in some regions.

For charged particles up to about 1 MeV electric and/or magnetic field can be used as a filter to separate out charged particles with specified energy, mass and charge. Different types of sensors are used for different energy ranges, e.g., solid state detectors (above ≈10 keV), channel electron multipliers/microchannel plates (below ≈100 keV), and retarding potential analysers (below ≈ 50 eV). Faraday cups can measure the total charge collected on the cup.

Electrostatic, magnetic or time-of-flight analysers have different characteristics (energy, angular, mass and temporal resolution). The instruments can give complete information of the distribution functions or only partial information. For spin stabilised spacecraft the rotation of the satellite is often used to get the pitch angle coverage. There are also sensors that can measure 2- or 3-dimensional distribution functions momentarily to obtain higher temporal resolution. Measurements of charged particles give in situ information on the local plasma as well as remote information on acceleration, precipitation and injection of plasma.

Instruments for detection of energetic neutral particles emitted from hot plasma regions have not been widely used in space plasmas. The technology exists, although the resolution of the instruments is not yet high (Gruntman, 1997, Barabash, 1995). The energetic neutral particle imaging technique is the only way to observe some regions of the magnetosphere remotely. This technique when fully developed can show the status of the magnetosphere in the same way as weather satellites follow the cloud coverage in the atmosphere.

Dosimeters measure integrated flux of radiation. The dosimeter does not give information on the type of radiation and often not on its temporal variation. If a filter is placed in front of the detector, different radiation types can be detected depending on the material of the filter and its thickness. The dosimeter can be of film type, but then the film needs to be developed. In space different electric components that are sensitive to radiation can be used as detectors.

3.1.2 Magnetic and electric field instruments

The plasma in space is most often collisionless which means that the charged particles do not interact directly with each other but through electric and magnetic fields. The magnetic field can be measured with a fluxgate magnetometer. The magnetometer is often mounted outside of the satellite main body to avoid disturbances from on-board current flows. The magnetic field measurements can be used to estimate current systems in the magnetosphere. The large-scale field-aligned current systems can be used to determine, e.g., the location of the auroral oval.

Magnetic field fluctuations (magnetic component of waves) can be measured with a search coil detector. Low-frequency waves can also be detected by a fluxgate magnetometer if the sampling rate is high enough. Waves can be good indicators of activity levels and the measurements are important for the understanding of physical processes in the magnetosphere or in interplanetary space.

Electric field measurements can be made with double probe technique or electron drift instruments. The frequency range from DC to above the electron cyclotron and plasma frequencies can be covered. The distance between the probes needs to be long enough (longer than the Debye length of the plasma). Long wires or booms, preferably along three axis perpendicular to each other, are needed. The electric field is estimated from the potential difference between the probes. The most common instrument is the Langmuir probe. The Langmuir probe, which is biased, measures the currents between probe and spacecraft or the potential difference between probe and spacecraft. Thus the spacecraft potential with respect to the surrounding environment and the plasma density (and temperature) can be estimated.

One can also use radio sounders. A radio wave is transmitted and it will be reflected at a density or turbulent layer. With this technique density gradients can be measured. In the outer magnetosphere signals between satellites can be used to scan the magnetospheric electron content.

3.1.3 Other instruments

When a spacecraft is charged one can actively neutralise the spacecraft with respect to the surrounding plasma potential. This can be made with ion or electron guns which cancel the potential difference (e.g., Oraevsky et al., 1992). This is done on scientific spacecraft to monitor low energy plasma and on spacecraft which have high solar panel voltages in a dense plasma. For example, the Charge Control System (CCS) measures and suppresses the large negative potential that can be built up on satellites in deep-space orbits. The CCS acts as a housekeeping device and keeps high altitude spacecraft from charging. An autonomous

charge control system that detects and mitigates dangerous charge build-up on spacecraft was successfully demonstrated on a USAF satellite.

The Austrian Research Center and an international scientific consortium have flown an ion emitter to control spacecraft potential on Geotail (Japanese), Interball (Russian) and Equator-S (Germany/NASA) (Schmidt et al., 1992). The mass of this emitter is 100-200 g with a life time of 2400-9600 hours at 10 mA and with a size less than 60 x 70 mm. On the sounding rocket CHARGE-2 the charging effects were studied for LEO satellites with the help of a fast-pulse electron gun (Raitt et al., 1992).

3.2 Specially designed space environment monitors

On-board the satellites in the USAF Defence Meteorological Satellite Program (DMSP) space environmental sensors (http://www.ngdc.noaa.gov/dmsp/descriptions/dmsp_sensors.html) are mounted. They are used for predictions. The three sensors are; a space plasma monitor (SSIES-2), an auroral particle sensor (SSJ/4), and a magnetometer (SSM). The data are used to make space weather forecasts (at the Falcon AFB Colorado) to help determine causes of satellite malfunctions as well as to provide warnings to satellite controllers and users when hazardous environmental conditions that could adversely affect satellite operations exist. The SSJ/4 instrument is designed to measure the flux of charged particles precipitating into the atmosphere. It consists of four electrostatic analysers for the energy range 30 eV to 30 keV. The topside ionospheric plasma monitor (SSIES) measures the thermal plasma. The sensors are tailored for the sun-synchronous orbit altitude of 840 km. The SSIES, SSIES2 and SSIES3 system contain an ion retarding potential analyser, an ion drift meter, a total ion trap and a spherical electron sensor. The SSIES3 also contains a plasma plate on the ion array for measuring the ionospheric electrons. In addition to the sensors for collection environmental data the three systems contain a sensor, SENPOT, measuring the electric potential between the plasma and the spacecraft. The sensor part of SENPOT is a section of the ion sensor aperture plane, which is electrically isolated from the spacecraft by 100 Mohms. The ion sensors are Faraday cups measuring thermal ions and Langmuir probes measure thermal electrons.

The Space Test Program at the Space and Missile Center (USA) together with Phillips Laboratory Geophysics Laboratory have developed the Compact Environmental Anomaly Sensor (CEASE) to monitor the environment. The instrument is developed to be autonomous, compact, light-weight and to consume low power. The instrument is designed to provide alerts when anomalies are expected to be caused by surface charging, deep dielectric charging, SEU or radiation dose effects. The instrument stores data up to 72 hours, which can

be transmitted down at request. The TSX-5 satellite is expected to be the first flight for CEASE. It is also planned for STRV-1C.

The Engineering Test Satellite-VI (ETS-VI), launched in August 1994, was equipped with a set of instruments to measure space environment effects (Goka et al., 1996a,b). The orbit had apogee at 7.1 Re, perigee at 2.2 Re and 13° inclination. National Space Development Agency of Japan (NASDA) built the satellite. The set of instruments, Technical Data Acquisition Equipment (TEDA), included; a heavy ion telescope, dosimeter, magnetometer, single event upset monitor, total dose monitor, solar cell radiation damage monitor, contamination monitor and electrostatic potential monitor.

On the Space Technology Research Vehicle (STRV-1B), launched in 1994 a Radiation Environment Monitor (REM) (Bühler et al., 1994) was flown to detect electrons and protons in a GTO orbit. REM was also flown 1994 in LEO on the space station MIR. The instrument was designed at the Paul Scherrer Institute (PSI) under an ESA contract. It has two Si detectors under shielding domes and detects electrons >1 MeV and protons >30 MeV (Bühler et al., 1996 a, b). The highest time resolution was 40 seconds binned into 16 detector channels. The GTO passes through the most severe parts of the proton and electron radiation belts. The proton dose variation showed some variation with active solar periods, as well as a general solar-cycle-related trend. An increasing trend in proton doses was suggested to be consistent with the anti-correlation expected for protons. The electron environment was found to be very dynamic. During disturbed periods the radiation belts correlate well with solar rotation and a clear seasonal pattern was seen. When a high-speed stream arrived, the energetic flux first showed a dropout and then an increase of the flux. For more information on REM results see, e.g., Daly (1998), Bühler et al., (1997), Bühler et al. (1998).

An improved version of REM is the Standard Radiation Environment Monitor (SREM) (Vuilleumier, 1997) which is developed and manufactured by Oerlikon-Contraves Space in co-operation with the Paul Scherrer Institute (PSI) under an ESA contract. The first SREM model is schedule for flight 1999 on STRV-1C and later on ESA satellites such as Integral and Rosetta. The instrument is calibrated with protons up to 600 MeV and electrons 5 MeV. One difference compared with the REM is that the problem with contamination of electrons in the high-energy proton channels is removed by a telescope configuration (Bühler et al., 1996a). The particle detectors measure electrons (0.3 - 6 MeV) and ions (8 - 300 MeV) in fifteen energy bands. The instrument has two alarms for high/low dose rates, dead-time correction for alarm, detection of SEE, total radiation dosimeter, and a large memory. SREM is contained in a box with the size 10 x 12 x 22 cm, weight ≤ 2.5 kg, and power consumption < 2 W.

An integrated environmental monitoring system is developed for several commercial satellites, e.g., on Martin Marietta spacecraft (Bogorad et al., 1995) and Lockheed Martin Astrospace (Intelsat VIII/VIIIA) (Ozkul et al., 1996). The system contains two sensors, a Surface Charge Monitor consisting of a 2 x 2 inch plate, where the potential difference is measured and a Dosimeter/Internal Charge Monitor. The surface charge monitor is designed to respond to electrons with energies from 5 to 20 keV. On INTELSAT VII/VIIIA two sets of plates are included, one looking away from Earth and the other towards north or south. The dosimeter/internal charge monitor consists of radiation sensitive p-FET integrated dosimeter devices with different thickness of the shielding. The p-FET device is sensitive to electrons with energies from 200 keV to 6 MeV but does not provide particle species or energy discrimination. The main components of the dosimeters are designed, manufactured and tested at the Center for Space Microelectronics Technology, Jet Propulsion Laboratory, California Institute of Technology. The total weight of the instrument is less than 0.5 kg and the power consumption about 0.5 W.

4 Non-local environment data

A spacecraft can monitor the local environment. This is the most accurate way to determine the causes of anomalies or to gain knowledge of hazardous events. Environment monitors on other spacecraft or ground-based systems are, however, sometimes needed for forecasts.

4.1 Ground-based environment data

Many indices, Kp, Dst, etc, have been created from measurements using ground-based magnetometers. They indicate the level of activity in the magnetosphere. The magnetometers are globally distributed, but due to the often remote locations and sometimes old techniques all magnetometers data are not available in real-time. Some of these indices can therefore be delayed several months. Near real-time information is, however, available from several stations and also for some indices (see, e.g., www.sel.noaa.gov). Using information of solar activity or solar wind characteristics to forecast these indices has been proven successful.

Geomagnetic disturbances can be monitored by ground-based magnetic observatories recording the three magnetic field components. The Kp index is obtained as the mean value of the disturbance levels in the two horizontal field components, observed at 13 selected, subauroral stations. The Dst index monitors the variations of the globally symmetrical ring current, which encircles the Earth close to the magnetic equator in the radiation belt of the magnetosphere. Hourly Dst indices since 1957 have been derived by Sugiura and his co-workers at the NASA Goddard Space Flight Center and the World Data Center in Kyoto, Japan. More information on geomagnetic indices can be found, e.g., on internet (http://nssdc.gsfc.nasa.gov/space/model/solar/geomagnetic_indices.html).

There are many ionosondes, riometers and radars that provide near-real-time information on ionospheric conditions. Cosmic ray data can be found on internet, e.g., (http://www.ngdc.noaa.gov/stp/SOLAR/COSMIC_RAYS/cosmic.html)

The sunspot number index is a measure of the area of the solar surface covered by sun spots and is often used as a solar activity index. The sunspot number is also called the Wolf number in reference to the Swiss astronomer J. R. Wolf who introduced this index in 1848. Yearly sunspot numbers are available since the telescope was invented in 1610. Another measure of solar activity, closely correlated with sunspot number, is the solar radio flux from the entire solar disk at a frequency 2800 MHz (10.7 cm). The radio flux has been recorded routinely by radio telescope near Ottawa since February 1947. Often used names for this index are F10.7 and Covington index.

4.2 Environment data from spacecraft

IMP (via OMNIWEB), GOES (via NOAA), and Meteosat/SEM 2, ISEE-1 and ISEE-2, REM on STRV and MIR, CRRES/MEA, AZUR/EI-88, SAMPEX/PET, and UARS/HEPS data basically contain flux values of ions or electrons for given energy ranges, dates and locations. Los Alamos National Laboratory (LANL) Geostationary Energetic Particle Data contain information from about 12 satellites measuring at geostationary orbit since 1976. LANL typically receives data from 3-4 satellites simultaneously. Data from the LEO spacecraft series DMSP can be accessed at request.

An observable change in the solar corona that occurs on a time scale between a few minutes and several hours and involves the appearance of a new, discrete, bright white-light feature in the coronograph field of view is called coronal mass ejection. The largest geomagnetic storms are caused by coronal mass ejections (http://www.sec.noaa.gov/today.html).

One of several models to forecast the space weather is the Lund Space Weather Model (LSWM). This model consists of different modules, each forecasting a space weather parameter at a specific time ahead. The model is based on intelligent hybrid systems, which combines both AI-methods such as neural networks and statistical and theoretical models. A so called “Sun Weather Viewer” has recently been developed. The Viewer downloads solar data in real-time, such as SOHO data, analysis and displays it. Solar magnetograms are downloaded, the coronal magnetic field is then computed and displayed in WWW environment. From the computations are also the heliospheric current sheet derived and displayed. The LSWM will be implemented in Java for real-time forecasts and interpretation of the space weather. The LSWM will play as a guideline for the developing of the generic tools for space environment analysis.

5 Local and non-local data

5.1 SPEE-WP210 and SPEE-WP220

In two separate work packages, SPEE-WP210 and SPEE-WP220, the correlation between anomalies on GEO satellites and local and non-local environment data have been studied. Local data are here defined as measurements made on-board the spacecraft. Non-local data include Kp, Dst, and energetic electron flux from other satellites (here GOES). The possibility to forecast anomalies on GEO spacecraft from the environment data has been investigated in both studies. The types of anomalies in these studies were not the most severe types. To get good statistics anomalies such as command counter reset, radiometer switch off, etc. were used. For more details see the technical reports from these work packages.

In SPEE-WP210 the satellite Meteosat-3 was studied together with electron fluxes measured by the on-board SEM-2 instrument (Rodgers, 1991, 1997). More than 700 anomalies from 7 years of the mission were used in the analysis. Meteosat-3 was launched during solar maximum and the mission ended at solar minimum (not a full solar cycle). The maximum electron fluxes (43 - 300 keV) measured by the SEM-2 instrument did not change between minimum and maximum. However, the length of periods with high fluxes and the dynamics changed during the mission.

The anomalies often occur after a period of high electron fluxes. The statistical difference between a time period preceding a non-anomaly and a period preceding an anomaly is, however, less than the variability of the electron fluxes that the satellite encounters due to asymmetries (in local time) in the magnetospheric particle populations. The Meteosat-3 anomalies and the electron fluxes (from each individual energy bin in the SEM-2 instrument) were used to generate an input data set with a time resolution of two hours. Neural networks were implemented to forecast the anomalies. For each of the five energy bins four flux values were used; the 2-hour mean flux, the maximum flux during the 2-hour period, the minimum flux during the 2 hours and an average flux from the 72 previous hours (3 days). Three data combinations were used; one with all five energy bins plus information on the spectral shape, giving 24 inputs for each 2-hour step (referred to as "_all"), one using the three highest energy bins (giving 12 inputs), and one the three lowest.

In WP210 a principal component analysis (PCA) was introduced. From this the three largest (in variance) coordinates (linear combination of the original data) were used in the forecast models.

The desired output was set to zero if no anomaly occurred and one if an anomaly occurred within the time window. The time window is selected to give a warning to a spacecraft

operator as early as possible without giving to many false alarms. Statistically, an anomaly occurred every fifth day. The time window was set to forecast anomalies 24 hours ahead.

Table 2. *All different combinations of the PCA file used in this report.*

name	resolution (h)	number of PCA components used	total number of columns	length of time window (h)
pa2	6	3	9	24
pa3	24	3	9	48
pa5	6	4	12	20
pa6	12	6	18	54
pa7	24	6	18	144

The neural networks were trained with a back-propagation learning algorithm. The output of a back-propagation network is a real number. A threshold must therefore be selected. The threshold was chosen so that the success of forecasting non-anomaly is about 80% or better.

Different networks were tested (in WP210) with different combinations of time windows corresponding to 32, 64, and 128 points (wa32, wa64, and wa128) together with the files described in Table 2. The information on the dynamics of the electron fluxes did not improve the result of the forecast. The selection of the lower, higher or all energy bins from SEM-2 gave more or less the same result. When the threshold was selected to forecast 83% of the non-anomalies, the warnings were forecasted with a success rate of 43% (forecasting 53% of the anomalies).

Further analysis showed that the forecasted anomalies were associated with high electron fluxes. We trained and tested a new network using 20% of the anomalies that occurred within 24 hours after the maximum observed electron fluxes. This gave the result that more than 92% of the anomalies at the time of high electron fluxes could be forecasted. The rest of the anomalies were used in another neural network but still only the anomalies associated with high electron fluxes could be forecasted. This led to the conclusion that half of the anomalies on Meteosat-3 could not be forecasted with the input parameters that were used.

There were some indications that some anomaly types are easier to forecast than others but no firm conclusion could be made from our study. The different local time sectors were also investigated. The forecasted anomalies are predominant in the morning sector but the anomalies that were not forecasted were more evenly distributed.

In SPEE-WP220 both Meteosat-3 and Tele-X satellite anomalies were used. The input parameters included relativistic electron flux (>2 MeV) and geomagnetic indices Dst and Kp. The relativistic electron flux data were read from the NOAA GOES space environment monitor CD-ROM and were selected from the measurements made by GOES-6, GOES-7, and GOES-8. The forecasts were made one day ahead with daily resolution of input data. It was found that time-delay neural network and learning vector quantization network both are well suited for the forecast task. Both networks gave similar forecast accuracy. Nevertheless, time-delay neural network gives a more stable performance than does learning vector quantization network. The parameters Kp and Dst gave good results in forecasting satellite anomalies. Relativistic electron flux (> 2MeV) provided less good results in comparison. This suggests that the electron flux with lower energy could be an important factor responsible for anomalies. With Kp as the input, the total prediction rate is about 80% at highest for events on Meteosat-3, the corresponding prediction rate for anomalies is 78% and for non-anomalies is 80%. Despite technology differences it was shown that a network trained to predict Meteosat anomalies could be applied to predict Tele-X anomalies provided that a threshold value is modified to account for the different susceptibility of the satellites. The success of prediction was 65% for both anomalies and non-anomalies.

5.2 Combination of local and non-local data

The data set created for SPEE-WP210 was combined with Kp and Dst data. Both Meteosat-3 and Tele-X anomalies were analysed, mainly for the time period when both satellites were operational.

Table 3 shows the results from different combinations of input data. The data are treated in the same way as in SPEE-WP210. The first column shows the number of the test, the second how the data are combined (the “level” the value for the selection of the anomalies directly associated with high fluxes, information on size of the input and output (net) and the size of the back propagation network (PE)). The last four columns show the results of four different trained networks; trained on Meteosat-3, Tele-X, the fiI (the Meteosat-3 anomalies that are associated with the highest electron fluxes preceding the anomaly using “level”) and fiII (the rest of the Meteosat-3 anomalies). In each column the result from the test file for each training file and also the network tested on all Meteosat-3 (me) and Tele-X (te) data are presented as the success of forecasting the anomalies (top value %) when the non-anomaly is well (about 80%) forecasted (bottom value %). In row 10 to 17 the networks trained to forecast Tele-X and Meteosat anomalies are tested on Meteosat-3 data for the full time period and for the period with only Tele-X data.

No difference between low and high energies in forecasting anomalies could be seen in SPEE-WP210. Therefore, this study used all energy bins (_all) in all examples. In row 1 only the electron fluxes at the time of forecast, 24, and 48 hours before (pa3) were used as input. The total number of anomalies on Tele-X is less than on Meteosat-3 but the success rate forecasting anomalies on Tele-X is 10-20% higher than on Meteosat-3. A network trained on Tele-X anomalies and tested on Meteosat-3 data (for the same time period as Tele-X) gave a success rate that was almost as good as when trained on Meteosat-3 anomalies (bold face numbers in Table).

In SPEE-WP210 the dynamics of the electron fluxes were used as input but with rather poor forecast results. A similar test is presented in row 2 again with an even less good result.

The Kp index was used to forecast anomalies on the satellite in SPEE-WP220. For this test we made the data set slightly different in order to combine the Kp index to the data set created in SPEE-WP210. The Kp index was interpolated to match the 2-hours resolution of the data set. In row 3 ten values of the Kp-index was used as input to the neural network. The ten values were selected from the time of forecast and the 9 previous values with twelve-hour time steps. This is indicated as Kp 10x12 in the table. Comparing row 3 with row 1 the success rate is about equal, the electron fluxes from the Meteosat-3 satellite are almost as good to use for forecasting as the Kp-index. This is not surprising since the Kp-index is an indicator of the level of geomagnetic activity.

Dst was tested in the same way as Kp. The results are shown in row 4. It can be seen that as in SPEE-WP220-TN Kp gives a better forecast than Dst.

Table 3 also shows the result using the electron fluxes measured on the Meteosat-3 combined with the Kp and Dst indices with different resolutions (rows 5 - 9 and 13 - 15). The improvement compared to row 1, 3 and 4 is approximately 5 %.

Table 3. *Prediction results of anomalies on Meteosat-3 and the Tele-X. Different data sets and back propagation networks have been used. The numbers show the success rate in percentages for anomalies (top value in each box) and non-anomalies (lower value). See text for further details.*

	Training file	**Meteosat-3**		**Tele-X**			**FiI Meteosat-3**			**fiII Meteosat-3**		
	Test file	**test**	**me**	**test**	**te**	**me**	**test**	**me**	**te**	**test**	**me**	**te**
	File comb.											
1	pa3 _all	**41**	**40**	**60**	54	**39**	94	26	38	50	59	72
	level.96 net9+1 PE6+2	**88**	**88**	**87**	86	**89**	94	94	92	72	73	70
2	wa64 _all	40	39	44	43	37	71	34	37	30	33	33
	level.96 net15+1 PE8+2	77	79	77	77	79	82	83	81	82	83	80
3	Kp 10x12 (_all)	60	42	65	65	49	85	23	30	31	33	34
	level.96 net10+1 PE5+2	78	88	79	79	82	94	96	94	87	88	85
4	Dst 10x12 (_all)	53	35	62	61	48	88	24	30	14	15	16
	level.96 net10+1 PE5+2	77	89	78	78	81	94	95	92	94	94	93
5	pa3 dst 3x24 _all	54	41	68	51	34	96	22	31	38	41	48
	level.96 net12+1 PE6+2	80	89	82	89	91	95	96	94	82	84	80
6	pa3 kp 3x24 _all	55	53	67	53	36	92	24	34	47	49	55
	level.96 net12+1 PE6+2	81	81	79	88	91	96	96	94	75	76	73
7	pa3 wa64 kp+dst 10x12 _all	47	49	64	67	40	92	21	28	38	40	44
	level.96 net44+1 PE20+10	87	87	86	85	87	98	96	94	85	86	82
8	pa3 Kp 4x12 _all	54	54	71	69	50	94	23	30	25	23	28
	level.96 net13+1 PE8+3	80	80	80	80	83	97	97	94	91	92	90
9	pa7 Kp 10x12 _all	51	53	71	76	46	97	34	47	41	39	41
	level.95 net28+1 PE14+7	79	78	79	79	78	88	89	88	80	80	78
10	pa3 month(1/2 year) _all	47	47	60	71	49/52	88	41	59	37	36	38
	level.95 net10+1 PE5+2	80	79	88	76	77/80	94	82	83	79	81	80
11	pa3 year _all	47	41	63	75	44/51	86	42	55	45	49	45
	level.95 net10+1 PE5+2	80	81	87	78	82/82	93	84	85	76	79	87
12	pa3 hour _all	50	50/51	54	66	50/46	95	42	61	32	33	40
	level.95 net10+1 PE5+2	79	77/81	89	78	82/80	85	82	82	82	85	83
13	pa3 _all	47	48/40	60	70	50/52	95	42	60	38	37	41
	level.95 net9+1 PE5+2	81	80/83	87	76	76/80	84	81	81	78	80	80
14	pa3 4x6 Kp _all	50	51/51	59	67	49/51	96	44	60	45	40	41
	level.95 net13+1 PE5+2	79	78/82	87	78	79/82	83	81	82	77	78	78
15	pa3 4x12 Kp _all	51	51/51	61	70	51/53	98	44	60	41	41	41
	level.95 net13+1 PE5+2	78	78/82	86	76	77/80	83	82	82	79	80	78
16	pa3 4x18Kp+Dst hh mm yy	**57**	58/51	**69**	79	38/37	**96**	**46**	**63**	54	50	41
	level.95 net20+1 PE5+2	**78**	78/83	**85**	78	86/88	**88**	**81**	**80**	74	74	82
17	pa3 4x18Kp+Dst hh mm yy	57	59/50	70	82	42/41	97	46	63	55		51
	level.95 net20+1 PE10+4	78	78/84	85	79	83/87	88	81	80	74		82
18	1 output=Meteosat+Tele-X	62	63				76	58		38	62	
	All the rest as test 16	79	80				85	81		87	79	
19	as test 16 + time since last	52	53				95	43		48	43	
	Meteosat anomaly	81	80				89	83		77	78	
	level.95 net18+1 PE5+2											

Daily, seasonal and solar cycle dependencies of the anomaly occurrence frequency have also been tested for both Meteosat-3 and Tele-X. In row 10 the year has been divided into two periods centred around the equinoxes, giving a 6-month period. The input to the network is the electron flux from pa3 (see Table 2) together with the 6-month-index. Splitting the year into two halves does not improve the result. The network trained with Tele-X anomalies and tested with the Meteosat-3 time series is given for two cases. The first is when all seven years of the mission are used, the second for only the period covered by Tele-X data (four years). The higher occurrence rate at the equinox is seen already in the electron data.

The phase of the solar cycle was introduced as a value ranging from 0 (1988) to 7 (the end of the Meteosat-3 mission). The network was trained (row 11) with Tele-X anomalies and for phase values greater than 4. The Meteosat-3 data was tested with the full seven-year period.

Comparisons using information on the local time are difficult since the two satellites were not at the same location and Meteosat-3 was moved several times. We used UT instead of the local time in row 12. Again the variability of anomaly occurrence with respect to local time exist already in the electron flux data from Meteosat-3.

In row 16 and 17, all data above (expect the dynamics of the electron fluxes) are used as input for the forecast. The result is 10% better both for Meteosat-3 and Tele-X (compare row 1 and 16). In Figure 1 the result of the four different networks from row 16 are shown. The time period in the Figure 1 correspond to the time when both satellites were operational. The four curves in a panel are the output, from the bottom the Meteosat-3, Tele-X, fiI and fiII of the trained networks. At the top of each panel the anomaly times for Meteosat-3 (lower) and Tele-X are shown.

In row 18 the input to the network is the same as in row 16 but the output is a combination of Meteosat-3 and Tele-X. The output is one (1) if one of the two satellites had an anomaly within 24 hours otherwise zero (0). The result is similar to row 16. The statistics has changed, but the anomalies that previously were not predicted are still not predicted.

The last test (row 19) was made to see if the forecast is improved by including information about when the previous anomaly occurred. Wrenn and Sims (1993) have suggested that for deep dielectric charging the successive switching is about 30 hours. The test did not improve the forecast of Meteosat-3 anomalies.

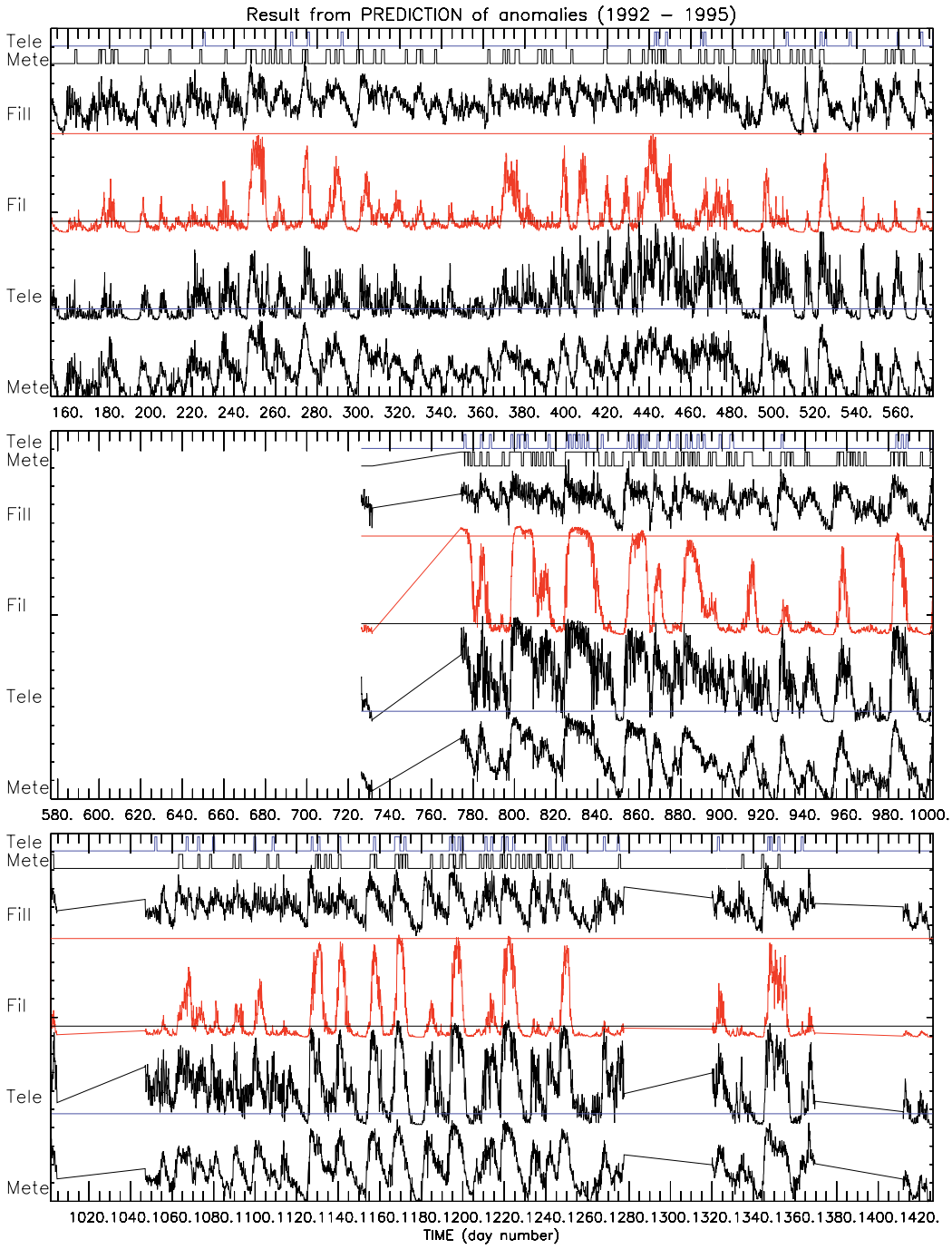

Figure 1. *The result from the test (row 16, Table 3). The time series covers 1992 to 1995. There were time gaps when the SEM-2 was not operated. From bottom the output result from the network trained with; Meteosat-3 , Tele-X, fiI and fiII are plotted. At the top are the anomalies from Meteosat-3 and Tele-X represented as a squared line. The square lines have one day resolution and the anomaly occurred at the end of the block.*

5.3 Discussion

The forecast efficiency was not found to depend on the choice of energy bin in the energy range 40 keV to 300 keV. The neural network could only find the anomalies that were associated with high fluxes independently of the energy (within this energy range). The input data were selected from period of times before the forecast. These data were tested with different configuration for instance last measurement, 12 hours and 24 hours before. When testing the different combinations three measurements were found to be enough to make good forecast, no particular combination was found to be better.

Wrenn (1995) and Wrenn and Sims (1996) analysed anomalies on the DRA δ satellite together with electron fluxes from GOES (>2 MeV) and Meteosat-3 (>0.2 MeV). The time period was March 1991 to March 1994. The anomalies on DRA δ was of same kind as the anomalies that we have studied. There was a clear correlation between the anomalies on DRA δ and the high electron fluxes observed during several days preceding the anomaly time. The electron fluxes from GOES and Meteosat-3 were used to calculated the fluence behind a layer, equivalent to a shield <1.5 mm Al. At the time of anomaly the satellite had been exposed to a fluence above 10^{11} MeV cm^{-2}. This is enough to cause deep dielectric charging. The anomalies were observed between 6 and 12 local time which indicates the same cause. The result of the study in SPEE-WP210 shows that the anomalies in Meteosat-3 are associated with high fluxes, independent of the electron energy (for the energy range covered by the measurements). One can thus assume that the anomalies that are forecasted with the neural network are associated with high fluxes at least in the energy range 43 keV to above 2 MeV. This suggests that anomalies are caused by deep dielectric charging. There are also reasons to believe that the flux of electrons below 43 keV is increased, therefore deep dielectric charging is not necessarily the only possible cause. Also surface charging can cause or contribute to some of the anomalies.

Surface charging on LEO spacecraft is correlated with solar activity (Frooninckx and Sojka, 1992). Solar minimum conditions favour spacecraft charging more frequently and to higher values due to a lower local plasma density.

Deep dielectric charging is usually occurring between 6 and 12 local time and surface charging mainly between 22 and 8 local time. Table 4 shows the result from SPEE-WP210. The number of warnings for each local time sector is presented. The next column shows the number of anomalies that are correctly forecasted and is followed by the number of anomalies that are not correctly forecasted. Two cases with 1 point (anomaly within 2 hours) and 12 point warning (anomaly within 24 hours) are shown. As concluded in SPEE-WP210 the anomalies not forecasted are more evenly distributed in local time. The highest numbers of forecasted anomalies are between 2 and 10 local time. The local time pattern for surface

charging only exists during active periods according to Wrenn and Sims (1993). During quiet times, anomalies are evenly distributed throughout the day.

Table 4. *Data from Table 11 (SPEE-WP210). The level in this example was set to 0.5. Therefore the success rate of the non-anomalies is not optimised to 80%, but higher. This gives the success rate of approximately 30% for warnings. This table is only used to identify the tendency of the forecast.*

local time	12 point warning	predicted	not predicted	1 point warning	predicted	not predicted
22-24	489	93	**396**	51	17	**34**
0-2	435	91	344	50	18	32
2-4	**551**	**259**	292	**64**	**44**	**20**
4-6	556	195	361	61	35	26
6-8	509	148	361	60	30	30
8-10	526	184	342	62	30	32
10-12	393	83	310	44	12	32
12-14	336	**67**	269	34	**6**	28
14-16	**327**	82	**245**	**33**	12	21
16-18	342	68	274	37	9	28
18-20	348	80	268	35	7	28
20-22	367	81	286	39	11	28
average value	432	119	312	48	19	28

In Figure 2 the results from a neural network trained with anomalies from Meteosat-3 that are associated with high electron fluxes (fiI) from test presented in row 16 are shown. Out of the four different anomaly sets (Figure 1) this set gives the clearest output signal varying between 0 and 1. In addition to the output signal from one of the networks is the Kp-index and the Dst-index given in the figure. The anomalies on-board Meteosat-3 and Tele-X are also included as squared lines. DRA δ anomalies from Table 2 in Wrenn (1995) have also been included.

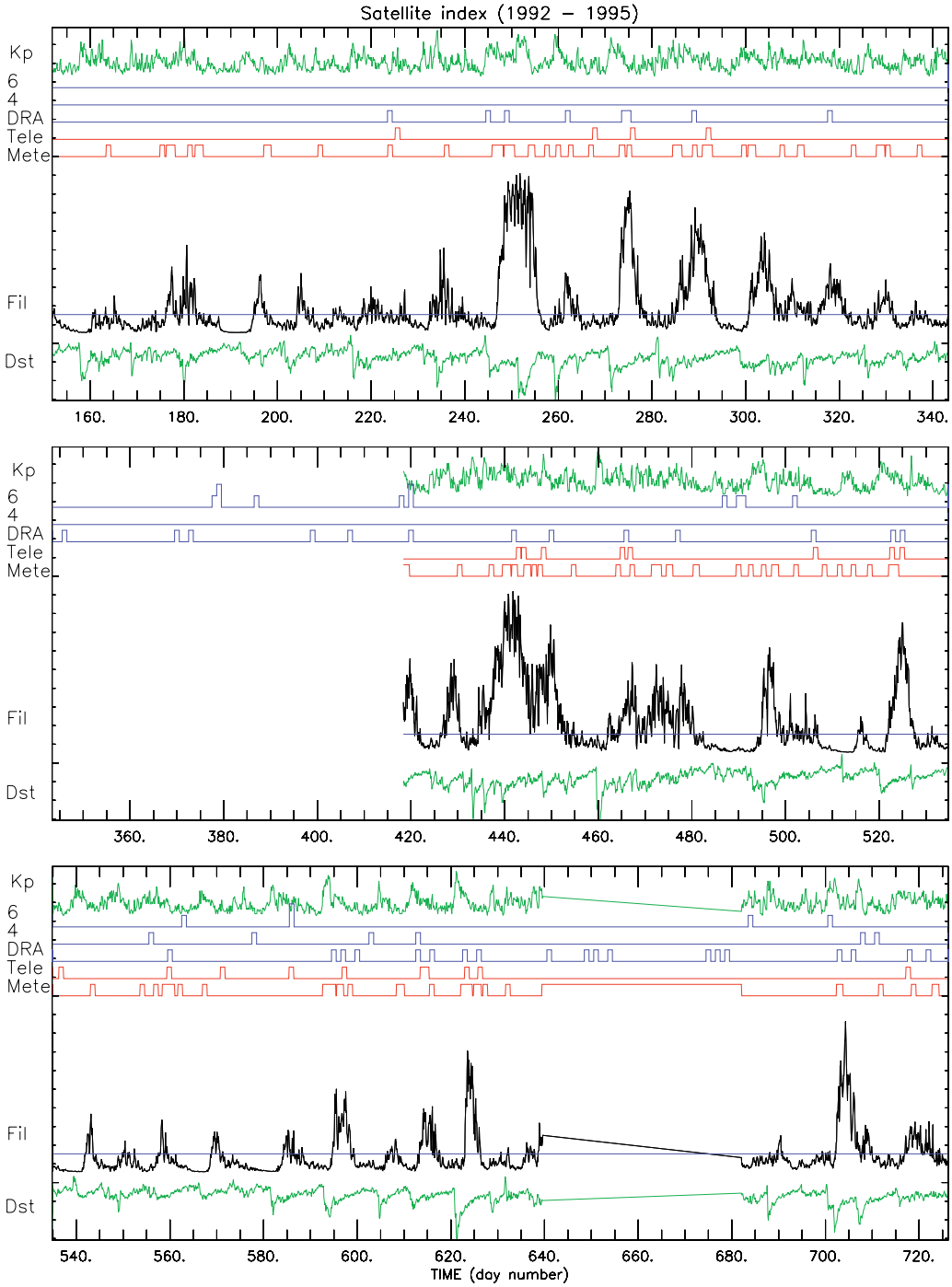

Figure 2. *Network trained with fiII is plotted again. Dst is shown in the bottom of the panel and the Kp-index at the top. The squared lines in the figure show anomalies from Meteosat-3, Tele-X, DRA-δ, reported environmental, and other anomalies. The anomalies for Meteosat-3 and Tele-X occurred at the end of each block while for the others the anomaly can occur any time in the block. The time of the anomalies on DRA-δ is from Table 2 in Wrenn, 1995 and cover only 1992 to March 1994. The other reported anomalies are from Goddard spacecraft yearly reports 1993, 1994 and 1995.*

When anomalies on Tele-X were used to train a neural network, only test data from solar minimum conditions were used. When anomalies from Meteosat-3 were tested with the network, the same result was obtained if only the same period as Tele-X or the full Meteosat-3 period was used. The increase of electron flux during several days is more pronounced near solar minimum (Wrenn and Sims, 1996), this can be seen in Figure 9 in SPEE-WP210. For Meteosat-3 the number of anomalies increases with time. The neural network that was trained with Tele-X anomalies was tested with Meteosat-3 anomalies from the same 4 years and the full 7-year period. The test result forecasting Meteosat-3 anomalies was the same using both time periods. This implies that a solar cycle dependence exists in the environment data but the increased number of anomalies could also be due to ageing effects. It would be interesting to look at a satellite covering a period from solar minimum to solar maximum or longer to compare the solar cycle effects with ageing effects.

6 Summary

For Meteosat-3 and Tele-X 50 to 60 % of the anomalies were possible to forecast. They were found to be associated with increased electron fluxes. These high-energy particles cause deep dielectric charging. All anomalies do not have that cause. Electrons of low energies (below 30 keV) have not been used and therefore some surface charging anomalies are most likely missed. SEU can not easily be monitored and the percentages of anomalies due to SEU is not established.

In Figure 2 the anomalies on Meteosat-3 and Tele-X together with anomaly data (DRA-δ) from the literature are presented together with output from one of the neural networks. The anomalies from the three satellites are forecasted reasonably well.

Also anomalies reported from Goddard spacecraft were plotted in the figure. We only used the anomalies they classify as environmentally caused and unknown. The majority of environmentally caused anomalies are claimed to be single event upsets. Both categories reported by the Goddard spacecraft control are of more severe nature than, e.g., command counter resets but still not dangerous for the mission. In Figure 2, the Goddard anomalies are not as well forecasted with the neural network as the anomalies on the other three satellites.

The forecasted anomalies on Meteosat-3 have the same local time dependence as found by Rodgers (1991). These morning anomalies were associated with charge accumulation of less than 3 days with a burst of high fluxes as trigger (electrons > 200 keV). This seems also to be the case for anomalies that are forecasted in this study on Meteosat-3 and Tele-X. The un-forecasted anomalies (Table 4) indicate a peak for Meteosat-3 at midnight. These could be the same as Rodgers (1991) claimed to be associated with a charge accumulation of 8 days with unknown trigger mechanism. In the forecast model these anomalies were not well forecasted and no clear environment factor was found.

Wrenn (1995) concluded “Comparison between ANIK and DRA-δ might suggest that the higher the threshold, the fewer the discharges, but that when one does occur it will be larger and much more damaging; the chance of this happening increases with mission duration.”

6.1 Monitor performance

The environment a satellite is exposed to is usually varying greatly during one orbit around the Earth. In SPEE-WP210 we showed that the time resolution to monitor the environment must be higher than the orbital period.

The analysis of spacecraft anomalies usually needs long time series (many years). On-board instruments should measure with high time resolution using pre-processing before transmitting the data down. One way to do this is to measure with high time resolution, calculate an average value and keep the lowest and highest value.

The SREM instrument has been described briefly in Section 3.2. It contains three particle detectors with high energy-resolution, an internal dosimeter, and makes internal temperature measurements. We have mainly studied anomalies associated with increased energetic electron fluxes. A high energy-resolution of the space monitor is not needed according to the results. There are, however, different types of anomalies so both the high-energy range (>2 MeV) and the lower energies 40-300 keV are most likely of interest. It has also been shown that these two energy ranges do not give a good solution for all anomalies. Spacecraft charging and associated discharges can also cause unwanted phenomena on a spacecraft, therefore should energies below 40 keV also be covered. A one-day-ahead forecast was the goal of the study, so that it can be used as a planning tool for satellite operators. With on-board "intelligence" some automatic systems could be defined, but such systems are outside the scope of this note. For post-event analysis an on-board autonomous system with higher time resolution would be preferred.

In LEO the effects by the SAA, and the northern and southern auroral ovals impact on electronic are often monitored. For an environmental monitor on-board GEO spacecraft the long-term changes of high-energy particles is of interest. Changes in magnetospheric and solar activity during the solar cycle should be monitored. A SEU monitor can be a memory chip that holds a pattern in the memory cells. A computer checks continuously how many bitflips that have occurred during the integration time and then resets the pattern. The memory cells that are selected for this type of monitor should be resistant to latch-up. Since the memory is being continuously reset, a latch-up that occurs does not influence the data too much.

An environmental monitor for commercial satellites could also use the concept of Bogorad et al. (1995); a dosimeter measuring energetic particles from about 80 keV for internal charging and one or several detectors measuring the surface charging (can either be a dosimeter in the energy range about 1-30 keV or a plate detector). Measurements of the surface charge can, however give the information to late. The dosimeter measure accumulated total dose and might not have the temporal resolution needed for good forecast possibilities. In this study the influence of the electron above 2 MeV was not strong but we still believe that it is important to cover this energy range. In addition a sensitive memory chip to monitor the SEU rate is recommended. The impact of protons is not studied, but a dosimeter measuring the high-

energy protons might help improving the understanding of the processes causing anomalies and to develop improved space weather monitors.

An environmental monitor must be able to survive the whole mission, although ground-based data can be used after the first part of the mission when the sensitivity to energetic particles is known. It is also shown that a fairly good forecast can be made using data from another spacecraft. There will, however, in the future also be other needs for a good knowledge about the space weather. A set of space weather monitors can therefore play a very important role, in the same sense as meteorological instantaneous and long time series data are for the climatology today. Also the knowledge about the space "climate" will be essential when more space based tools are being used and more manned spacecraft are being launched. The weight and power consumption of an environmental monitor must be kept low.

6.2 A satellite anomaly index

A spacecraft operator could use an index that gives a warning a reasonable time before an anomaly occurs and the index should not give too many false alarms. Satellite have different sensitivity to the environment. The interpretation of the index must therefore be adjustable to various spacecraft.

The index should give a warning when there is an increased risk of anomalies. Since there are different causes of anomalies, the index must take this into account. Different processes will also affect the spacecraft in different ways, so a single index might not be enough.

The forecast model in this study is sensitive to periods with high fluxes of energetic electrons. Thus, mainly the anomalies that are associated with deep dielectric charging are possible to forecast with the model.

The suggested forecast model is based on a 24-hour-ahead warning. It is developed to correctly forecast the non-anomalies with at least 80% success. The models that are stable with an easily distinguished difference between anomaly risk and no risk conditions have been selected. Using the energy flux only (SPEE-WP210) is not a good choice since the output of the model give an index frequently fluctuating between high and low values. Daily variations that are normally not causing problems are also influencing the results too much. The index that is easiest to read (has the largest difference between low and high value) is from the model trained with anomalies associated with high electron fluxes. This index indicates the presence of high fluxes of energetic electrons in geostationary orbit. It is not sensitive to the daily variations and can be used for several spacecraft.

The fraction of days when anomalies occurred is 19%. The selected forecast model gave warnings during about 23-24 % of the time for both Meteosat-3 and Tele-X. The model forecasted 46% (Meteosat-3) and 63% (Tele-X) of the desired warnings correctly. When the model gave a low index value it is correct up to 87% and 96%, respectively. The anomalies that the model does not forecast are probably caused by some other effect than high electron fluxes. Rodgers (1991) found anomalies that were correlated with high electron fluxes and another group that was not associated with a large peak in the energetic electron fluxes but instead with an accumulation time of several days. If the warnings should be better forecasted the threshold values could be changed but that will of course also change the number of false alarms.

In this report a forecast model is presented that can warn an operator when higher electron fluxes can cause anomalies on GEO satellites. For the satellites used in the test the model forecasted up to 70% of the anomalies. The model gave warnings about 25% of the time. Depending on the satellite sensitivity and selected threshold value, the model gives a correct warning 22 to 36 % of the time.

6.3 Summary of spacecraft anomalies

The anomalies are not randomly distributed. There are seasonal peaks near the equinoxes. There is also a peak over the SAA (for low-altitude Earth orbiting spacecraft) where the inner radiation belt extends to lower than usual altitudes. Coronal mass ejections and proton events are associated with anomalies. Some charging events have been associated with passage through regions connected to intense auroras.

Specifically for a low altitude polar orbiting spacecraft there is an increased risk:

– in intense auroras and in eclipse and when there is a drop in plasma density
– in the South-Atlantic anomaly
– around time of equinoxes
– near midnight
– when a magnetic storm is in progress.

For a spacecraft in GEO there is increased risk:

– near midnight for surface charging
– in daylight for internal discharges
– around time of equinoxes
– when Kp >4 (Koons and Gorney, 1991).

Anomalies may be significantly reduced by a proper design of the spacecraft. Although many anomalies are induced by natural causes, more and more “pollution” is causing problems in

the environment. There is an increase in fragments from launches and spacecraft failures, and there is significant electromagnetic pollution from space- and ground-based systems.

7 Conclusions

The charged particle environment depends on complicated coupling processes in the solar system. Advanced methods are therefore needed to properly model the conditions at different locations and with temporal resolution that is sufficient to handle the dynamics of the system. In order to be able to forecast an event or to have environmental data as input to the design of mission elements more advanced tools operating on a more complete database are needed. The present models and tools do not give enough detailed information on, e.g., the dynamics of the radiation environment. Today, there are environmental data available in more or less real time that can be used for near real-time forecast of parameters such as the Dst. Dst gives good information on the dynamics of the Earth's radiation belts and the ring current, regions that include the geostationary orbit. To be able to do these types of studies new tools have been developed based on neural network techniques. Forecasting proton events on longer time scales, such as months and years ahead, is a question of forecasting the solar activity. Also in this respect results from instruments on board SOHO, especially the MDI instrument, have dramatically changed our view on the Sun. The solar activity is caused by the changing magnetic field. Helioseismological studies have shown where the dynamo for the large scale solar magnetic field is located. The magnetic field can then be followed up through the convective zone to the photosphere and further out into the corona and interplanetary space. The evolution and distribution of the magnetic field during the solar cycle can now be understood as a combination of differential rotation, poleward motion and supergranular motion. Predicting the solar activity more accurately gives us methods to better forecast the proton events on longer time scales.

All spacecraft are effected by the space environment, but with different sensitivity. The spacecraft designers build the spacecraft to minimise the impact but must stay within allowed cost limits.

During operation the spacecraft operator learns how each individual satellite behaves. Directly after launch the satellites indicate many different types of anomalous behaviour, due to environment induced problems but also due to software and unexpected errors, conflicts between different on-board systems or malfunction of components. When the satellite behaviour has stabilised, minor anomalies that occur on the satellite are not always investigated. The operator can send up necessary commands to correct the satellite performance. Information of these events could be very valuable for anomaly studies. The use

of only the most spectacular anomalies or anomalies during the commissioning phase can make the results misleading for use on other spacecraft.

There are many examples of anomalies on interplanetary spacecraft and Earth orbiting satellites reported in the literature. The anomalies are from minor problems to total loss of satellites. The available database is, however, limited. An extensive European anomaly database is therefore needed.

A useful forecast tool must be based on data that are easily available in real-time. Space-borne monitors giving continuous data are few. Today SOHO and ACE spacecraft provide observations of solar activity and solar wind parameters. Data from these spacecraft have been very valuable for making new forecast tools that are available in real-time and also for the understanding of the physical processes that controls the space weather. It is important that these efforts continue and are complemented by other spacecraft to provide continuous observation of the solar activity also in the future.

More satellites equipped with environmental monitors to observe magnetospheric conditions are needed. The instruments provide information not only to spacecraft operators but can also be used for other purposes. New monitors under development and new techniques are being used for scientific investigations. Some of these newly developed instruments (high-energy electron telescopes, neutral particle imagers, etc.) are still not extensively tested in space but may become valuable for future space weather monitoring.

An environment monitor does not need very high-energy and temporal resolution but should cover a wide range of energies. All spacecraft should be equipped with environment monitors and the operators should keep records of anomalies. It can be a dosimeter, measuring some energy intervals between 40 keV - 10 MeV. A SEU detector should be included in GEO to give knowledge on effects by the cosmic rays and solar proton events. Since the Earth's magnetic field acts as a shield for cosmic rays, data from SEU detectors should be interesting to analyse.

Both measurements on-board a spacecraft and from ground-based locations can be used to forecast anomalies. About 50-70% of the anomalies seem to be fairly easy to forecast. In this study the forecasted anomalies were seen to be associated with high intensities of high-energy electrons (40-300 keV). This energy range can cause surface or deep dielectric charging.

One of the different forecast models has been used as a prototype of a satellite index that could be used by satellite operators as a warning for periods of time with higher risk to get anomalies on-board the satellite. The model gives a warning if an anomaly will occur within

the next 24 hours. 75% of the time covered by this study the model forecasted low activity, i.e., low risk of anomalies. When the model gave a warning that an anomaly will occur within 24 hours, it was correct for 22-36% of the events.

8 Acknowledgements

We wish to thank the ESA-TOS-EMA for initiating this project and their interest throughout its completion. Special thanks belong to the ESTEC Technical Officer Dr. Alain Hilgers and to Dr. Eamonn Daly whose comments and support were particularly useful.

9 References

Anderson, P.C., and H.C. Koons, Spacecraft charging on a low-altitude spacecraft in an aurora, J. of Spacecraft and Rockets, 33, 734, 1996.

Anselmo, J.C., Solar storm eyed as satellite killer, Aviation Week and Space Technology, p61, Jan. 27, 1997.

Baker D. N., J. H. Allen, R. D. Belian, J. B. Blake, S. G. Kanekal, B. Klecker, R. P. Lepping, X. Li, R. A. Mewaldt, K. Ogilvie, T. Onsager, G. D. Reeves, G. Rostoker, R. B. Sheldon, H. J. Singer, H. E. Spence, and N. Turner, An assessment of space environmental conditions during the recent Anik E1 spacecraft operation failure, ISTP Newsletter Vol 6, No. 2. June 1996.
http://www-istp.gsfc.nasa.gov/istp/newsletter.html

Baker, D.N., S. Kanekal, J.B.Blake, B.Klecker, and G. Rostoker, Satellite anomalies linked to electron increase in the magnetosphere, EOS, 75, 35, 1994.

Barabash S., Satellite observations of the plasma -neutral coupling near Mars and the Earth. IRF Scientific Report 228, Kiruna, 1995.

Bogorad, A., C. Bowman, A. Denis, J. Beck, D. Lang, R. Herschitz, M. Buehler, B. Blaes, and D. Martin, Integrated environmental monitoring system for spacecraft, JPL Technical Report.
http://www.jpl.nasa.gov/techreport/1995/95-0846.rfr.html

Buehler, P., S. Ljungfelt, A. Mchedlishvili, N. Schlumpf, A. Zehnder, L. Adams, E. Daly, and R. Nickson, REM, first year in space, 1994.
http://www1.psi.ch/www_lap_hn/ASTR_REM_JB94.HTML

Buhler P., L. Desorger, A. Zehnder, L. Adams, and E. Daly, Monitoring of the radiation belts with the raditation environment monitor REM, Radiation Belts: Models and Standards. Geophysical Monographs 97, American Geophysical Union, 265-267, 1996a.

Buhler P., A. Zehnder, L. Desorgher, W. Hajdas, E. Daly, and L. Adams, Simple instruments for continuous measurements of trapped particles, in Proceedings from "Environment Modelling for Space-based Applications," ESTEC, Noordwijk, NL, 18-20 September 1996b.

Buhler, P., A. Zehnder, L. Desorgher , W. Hajdas, E. Daly, L. Adams, Measurements of the Radiation Belts from MIR and STRV 1994-1997 http://www.estec.esa.nl/wmwww/wma/jan97/ieee97.html

Bühler P., A. Zehnder, L. Desorgher, W. Hajdas, E. Daly, Observation of Radiation-Belt Energetic Electrons with REM, 1998. http://www.estec.esa.nl/wmwww/wma/rem/sctc98/index.htm

Daly, E., and P. Nieminen, Solar Energetic Proton Events of 3-9 November 1997. http://www.estec.esa.nl/wmwww/wma/spe9711/

Daly, E., REM, 1998. http://www.estec.esa.nl/wmwww/wma/rem/

Daly, E.J, F. van Leeuwen, H.D.R. Evans, and M.A.C. Perryman, Radiation belt transient solar-magnetosphere effects on Hipparcos radiation background, IEEE Trans Nuc. Sci, NS41, 1994.

Frederickson, A. R., Radiation induced dielectric charging, in H.B. Gattett and C. P. Pike (Eds.) "Space Systems and Their Interactions with the Earth's Space Environment," Vol 71, pp. 386-412, American Institute of Aeronautics and Astronautics, Washington, DC, 1980.

Frooninckx T. B., and J. J. Sojka. Solar cycle dependence of spacecraft charging in low Earth orbit, J. Geophys. Res., 97, 2985-2996, 1992.

Gabriel, S. B., J. Feynman and G. Spitale, Solar Energetic Particle Events: Statistical Modelling and Prediction, in ESA Symposium Proceedings on "Environment Modelling for Space-based Applications", ESTEC Noordwijk, NL. 18-20 September 1996, SP-392, December 1996.

Garrett, H.B., The charging of spacecraft surfaces, Rev. of Geophys., 19, 577, 1981.

Garrett H. B., and A. C. Whittlesey, Spacecraft charging, an update, AIAA 96-0143, American Institute of Aeronautics and Astronautics, Washington, 1996. http://jpltrs.jpl.nasa.gov/1995/95-1568.pdf

Goddard Space Flight Center, Orbital anomalies in Goddard spacecraft for CY 1993, System reliability and safety office, code 302, Greenbelt, Maryland 20771, June 1994. http://arioch.gsfc.nasa.gov/302/oags.htm

Goka T., H. Matsumoto, T. Fukuda, and S. Takagi, Space environment and effect measurements from ETS-VI satellite, in Proceedings from "Environment Modelling for Space-based Applications," ESTEC, Noordwijk, NL, 18-20, 1996a.

Goka T., H. Matsumoto, T. Fukuda, and S. Takagi, Measurement of radiation belt particles with ETS-6 onboard dosimeter, in "Radiation Belts: Models and Standards" Geophysical Monograph 97, Eds Lemaire, Heynderickx, and Baker, AGU, pp. 251-254, 1996b.

Gruntman M., Energetic neutral atom imaging of space plasmas, Rev. Sci. Instrum., 68 (10), 1997.

Hastings, D., E., A review of plasma interactions with spacecraft in low Earth orbit, J. Geophys. Res., 100, 14457-14487, 1995.

James, B. F, O.W. Norton, and M.B. Alexander, The natural space environment: effects on spacecraft, NASA Ref. Pub. 1350, 2, 1994. http://trs.msfc.nasa.gov/mtrs/94/rp1350.pdf

Kalweit, C., Review of the status of spacecraft-charging studies, ESA Journal, 5, 75, 1981.

Koons, H.C., and D.J. Gorney, Relationship between electrostatic discharges on spacecraft P78-2 and the electron environment, J. Spacecraft, 28, 683, 1991.

Lauriente, M., and A.L. Vampola, Spacecraft anomalies due to radiation environment in space, NASDA/JAERI 2nd International Workshop on Radiation effects of Semiconductor Devices for Space Applications, Tokyo Japan, 1996. http://envnet.gsfc.nasa.gov/Papers/JPRadiation.html

Lauriente, M, A. L. Vampola, R. Koga, and R. Hosken. Spacecraft anomalies due to the radiation environment, AIAA 36 Aerospace Sciences Meeting Reno Nev. USA, 1998. http://envnet.gsfc.nasa.gov/Papers/Reno98.html

Lanzerotti L. J., C. Berglia, D. W. Maurer, G. K. Johnson, III, and C. G. Maclennan, Studies of spacecraft charging on a geosynchronous telecommunications satellite, Proceeding of the 1996 COSPAR conference.

Leach, R.D., and M.B. Alexander, Electronic systems failures and anomalies attributed to electromagnetic interference, Marshall Space Flight Center, NASA Reference Publication 1374, 1995.

Leung, P., A. C. Whittlesey, H. B. Garrett, and P. A. Robinson Jr., Environment-induced electrostatic discharges as the cause of Voyager 1 power-on resets, J. Spacecraft, 23, 3, 1986.

Oraevsky V. N., Yu. Ya. Ruzhin, and V.S. Dokukin, The dynamics of the object potential during electron beam injection and the possibility to control it, Adv. Space Res., 12, 1992.

Ozkul A., F. Scali, D. Liu, and C. Bowman, Design and operational characteristics of electrostatic charge measurement onboard Intelsat VIII & VIII-A communication satellites, Abstract ESA Symposium on Environmental Modelling for Space based Applications, 1996. http://www.estec.esa.nl/CONFANNOUN/96a09/Abstracts/abstract60/index.html

Raitt W.J., N. B. Myers, D. C. Thompson, P. M. Banks, B. E. Gilchrist, T. Neubert, P. R. Williamson, and S. Sasaki, Recent experimental measurements of space platform charging at LEO altitudes, Adv. Space Res., 12, 1992.

Reames, D. V., Solar energetic particles: A paradigm shift, Rev. Geophys. Vol. 33 Suppl, 1995.

Remez J. W., and H. C. McLeod, Orbital anomalies in Goddard spacecraft for calender year 1995, Goddard Space Flight Center, NASA technical paper, 1996. http://arioch.gsfc.nasa.gov/302/oags.htm

Robinson, P., W. Lee, R. Aguero, and S. Gabriel, Anomalies due to Single Event Upsets, J. Spacecraft and Rockets, Vol 31, 1994.

Rodgers, D.J., Correlation of METEOSAT-3 anomalies with data from the spacecraft environment monitor, Internal ESTEC working paper, no.1620, 1991.

Rodgers, D.J., A.J., Coates, and A.D. Johnstone, E.J. Daly, Correlation of METEOSAT-3 anomalies with data from the space environment monitor, in Proceedings of the Esa Workshop on Space Weather, WPP-ISS, Noordwijk, The Netherlands, 1999.

Schmidt, H. Arends, W. Riedler, K. Torkar, F. Rüdenauer, M. Fehringer, B. Maehlum, and B. Narheim, Energetic ion emission for active spacecraft control, Adv. Space Res., 12 no 12, 1992.

Selding P. B., Matra puzzled over Spanish satellite failure, Space News, January, 1998.

Standard radiation environment monitor (SREM), Oerlikon-contraves space, Marketing & Sales Department CH-8052 Zurich.

Stevens, N.J., and M.R. Jones, Comparison of auroral charging predictions to DMSP data, AIAA 95-0370 33rd Aerospace Sciences Meeting, 1995.

Tribble, A. C., The space environment, implications for spacecraft design, Princeton University Press, Chichester, West Sussex, 1995.

Vampola, A.L., Analysis of environmentally induced spacecraft anomalies, J. Spacecraft and Rockets, 31 (2), 164, 1994.

Violet, M.D., and A.R. Frederickson, Spacecraft anomalies on the CRRES satellite correlated with the environment and insulator samples, IEEE Trans on Nuclear Science, 40 (6), 1512, 1993.

Vuilleumier P., Standard radiation environment monitor (SREM) requirements specification, ESA Ref.: SREM/RS/002 Issue 8, 1997.

Walter B. T., Orbital anomalies in Goddard spacecraft for calendar year 1994, Goddard Space Flight Center, NASA technical paper 3636, 1995. http://arioch.gsfc.nasa.gov/302/oags.htm

Wilkinson, D.C., National Oceanic and Atmospheric Administration's spacecraft anomaly data base and examples of solar activity affecting spacecraft, J. Spacecraft and Rockets, 31 (2), 160, 1994.

Wrenn G. L., Conclusive evidence for internal di-electrical charging anomalies on geosynchronous communications spacecraft, J. Spacecraft and Rockets, 32 (3), 1995.

Wrenn G. L., and A. J. Sims, Surface charging on spacecraft in geosyncronous orbit, R. N. DeWitt et al. (eds.) "The Behaviour of Systems in the Space Environment," Kluwer Academic Publ., Netherlands, 491-511, 1993.

Wrenn G. L., and A. J. Sims, Internal charging in the outer zone and operational anomalies, in "Radiation Belts: Models and Standards," Geophysical monograph 97, AGU, 1996.

Appendix 1:

Some WEB addresses

Baker et al. An assessment of space environmental conditions during the recent Anik E1 spacecraft operational failure

http://www-istp.gsfc.nasa.gov/istp/newsletters/V6N2/newsletter.html#ANCH4

BATES Solar Flare Server

http://umbra.nascom.nasa.gov/batse/batse_years.html

Bogorad et al. Integrated environmental monitoring system for spacecraft

http://www.jpl.nasa.gov/techreport/1995/95-0846.rfr.html

Buehler et al. REM, First year in space

http://www1.psi.ch/www_lap_hn/ASTR_REM_JB94.HTML

Buehler et al. Multi-shielded p-FET dosimeter

http://www.jpl.nasa.gov/techreport/1995/95-0333.rfr.html

Bühler et al. Measurements of the radiation belts from MIR and STRV 1994-1997

http://www.estec.esa.nl/wmwww/wma/jan97/ieee97.html

Bühler et al. Observation of radiation-belt energetic electrons with REM

http://www.estec.esa.nl/wmwww/wma/rem/sctc98/index.htm

Charge Control system protects spacecraft from charging effects

http://www.plh.af.mil/Success/ccs.html

Daly and Nieminen Solar energetic proton events of 3-9 November 1997.

http://www.estec.esa.nl/wmwww/wma/spe9711

Daly, E. REM

http://www.estec.esa.nl/wmwww/wma/rem/

DMSP

http://www.ngdc.noaa.gov/dmsp/dmsp.html

DRAO 10cm Solar radio noise patrol

http://www.drao.nrc.ca/icarus/www/sol_home.shtml

EnviroNET

http://envnet.gsfc.nasa.gov

GOES

http://www.ngdc.noaa.gov:8080/production/html/GOES/index.html

Goddard Space Flight Center (orbital anomalies)

http://arioch.gsfc.nasa.gov/302/oags.htm

IRF-Kiruna

http://www.irf.se/irfk.html

James et al. The natural space environment: effects on spacecraft

http://trs.msfc.nasa.gov/mtrs/94/rp1350.pdf

K-index

http://www.sel.noaa.gov/planetary_k.html

Lauriente et al. Experimental validation of south atlantic anomaly motion using a two-dimensional cross-correlation technique

http://envnet.gsfc.nasa.gov/Papers/Brussels1.html

Lauriente et al. Spacecraft anomalies due to radiation environment in space

http://envnet.gsfc.nasa.gov/Papers/JPRadiation.html

Lauriente et al., 1998 Spacecraft anomalies due to the radiation environment

http://envnet.gsfc.nasa.gov/Papers/Reno98.html

Lund Space Weather Center

http://nastol.astro.lu.se/~henrik/spacew1.html

Meteoroids

http://www.imo.net

http://esapub.esrin.esa.it/pff/pffv7n1/drov7n1.htm

Neutron monitor

http://odysseus.uchicago.edu/NeutronMonitor/neutron.html

OMNIWeb

http://nssdc.gsfc.nasa.gov/omniweb/html/ow_data.html

Ozkul et al. Design and operational characteristics of electrostatic charge measurement onboard Intelsat VIII & VIII-A communication satellites

http://www.estec.esa.nl/CONFANNOUN/96a09/Abstracts/abstract60

Photovoltaic and Space Environment Effects

http://powerweb.lerc.nasa.gov/pvsee/index.html

SEEB Publications

http://satori2.lerc.nasa.gov/DOC/publications.html

Space and Missile Systems Center, Test and Evaluation Directorate (SMC/TE)

http://www.te.plk.af.mil

SPACECAST 2020 Technical Report

http://www.au.af.mil/Spacecast/TOC1.html

Spacecraft Charging (Garrett and Whittlesey)

http://jpltrs.jpl.nasa.gov/1995/95-1568.pdf

SPENVIS

http://www.spenvis.oma.be

Schneider, H.J. SREM - The ESA Standard Radiation Environment Monitor

http://esapub.esrin.esa.it/pff/pffv6n4/schv6n4.htm

Space weather from NOAA

http://www.sec.noaa.gov/today.html

Study of Plasma and Energetic Electron Environment and Effects

http://www.geo.fmi.fi/spee

Sunspot Index Data Center (SIDC)

http://www.oma.be/KSB-ORB/SIDC/index.html
Wells, N. et al. The STRV 1B Radiation Environment Monitor
http://esapub.esrin.esa.it/pff/pffv4n4/ppfwelnr4.htm

Institutet för rymdfysik

Swedish Institute of Space Physics

Swedish Institute of Space Physics
Box 812, SE- 981 28 Kiruna, SWEDEN
tel. +46-980-790 00, fax +46-980-790 50, e-post: irf@irf.se

www.irf.se